Finite-element analysis of periodic piezoelectric transducers

Sylvain Ballandras, Mikaël Wilm,[a] Paul-Francis Edoa, Abdelaziz Soufyane, and Vincent Laude
LPMO/CNRS-IMFC associé à l'Université de Franche-Comté, 32 avenue de l'Observatoire, 25044 Besançon Cedex, France

William Steichen and Raphaël Lardat
Thales Microsonics (TMX), 399 route des Crêtes, B.P. 232, 06904 Sophia-Antipolis Cedex, France

(Received 20 June 2002; accepted 6 October 2002)

The need for optimized acoustic transducers for the development of high-quality imaging probes requires efficient simulation tools providing reliable descriptions of the behavior of real devices. The purpose of this work is the implementation of a finite-element model for the simulation of periodic transducer arrays. By using the assumption of harmonic excitation, the harmonic admittance of the studied structure can be derived. It is then shown how the mutual admittance is deduced from this feature, allowing one to estimate the amount of cross-talk effects for a given periodic transducer. Computation results are reported for standard linear acoustic probes, 2-2 (one-dimensional periodic) and 1-3 (two-dimensional periodic) piezocomposite materials. In the case of 2-2 connectivity composites, a comparison between nonperiodic and periodic computations of the mutual admittance is conducted, from which the minimum number of periods for which periodic computations can be trustfully considered can be estimated. © *2003 American Institute of Physics.*
[DOI: 10.1063/1.1524711]

I. INTRODUCTION

Ultrasound transducers for acoustic imaging are now standard tools for medical diagnostics and nondestructive control. Technological developments in this field during tens of years have resulted in the production of very sensitive acoustic probes providing accurate measurements for a wide range of applications. Such technical improvements are also due to a strong effort in the modeling of the dynamical behavior of these transducers. One of the most popular models devoted to piezoelectric vibrators was proposed by Mason[1] in the early 60s. This approach consisted in a simplified model using a scalar representation of the electroacoustic vibration, which is very efficient in the prediction of vibrations of archetypal structures (plates, bars, etc).[2] But, since then, technical improvements have rendered the fabrication of devices more and more different than these archetypes, and many authors have proposed theoretical approaches that are better adapted to the simulation of structures with general geometries. In 1966, Lloyd and Redwood[3] investigated the possibility of modeling vibration modes of thin piezoelectric plates using the finite difference method. A few years later, Holland[4] proposed to apply the Rayleigh–Ritz approach to solve this kind of problem. At the same time, Tiersten,[5] Eerniess,[6] and Allik and Hugues[7] explored the capability of finite-element analysis (FEA) to simulate piezoelectric structures. Since these pioneer works, many authors have contributed to the development and improvement of the modeling of piezoelectric problems using FEA.[8–12]

Modern ultrasound arrays for medical imaging applications are mainly based on composite structures associating materials of various natures. The actuation principle generally consists in the vibration of a piezoelectric transducer (PZT) ridge glued on a backing, with one or two matching layers covered by a Mylar layer and possibly an acoustic lens. These transducers exhibit up to 192 single transducers for one-dimensional (1D) periodic probes or more than 64×64 transducers for two-dimensional (2D) periodic devices devoted to three-dimensional (3D) imaging. Devices based on piezocomposites have also been introduced to improve the characteristics of classical acoustic probes, and the new concept of the micromachined ultrasound transducer[13] gives rise to new opportunities in the development of high-density integrated imaging devices.

Although FEA has been extensively used to address classical 2D or 3D problems (i.e., single transducer devices or reduced size arrays), it has seldom been adapted to explicitly take into account periodicity.[14] However, it is a very efficient way to simulate acoustic imaging probes exhibiting a large number of elementary transducers as those currently used in medicine. The design of transducers requires powerful and flexible tools, that can accurately simulate complex arrangements of materials exhibiting acoustic and dielectric losses. Furthermore, the periodicity of the probes has to be taken into account to correctly predict their capability to convert bulk vibrations into acoustic radiation, avoiding any parasitic effects due to waveguiding along the array. The present work is devoted to the development of finite-element computation tools to address this problem. It is based on an harmonic analysis of the admittance (or impedance)[15] of piezoelectric transducers as used for medical imaging or nondestructive evaluation. Periodicity is taken into account using a standard periodic finite-element approach and Bloch wave expansion allowing one to rigorously establish the periodic boundary conditions. Computations are performed for different kinds of piezoelectric ultrasound transducers to illustrate the effi-

[a]Electronic mail: mikael.wilm@lpmo.edu

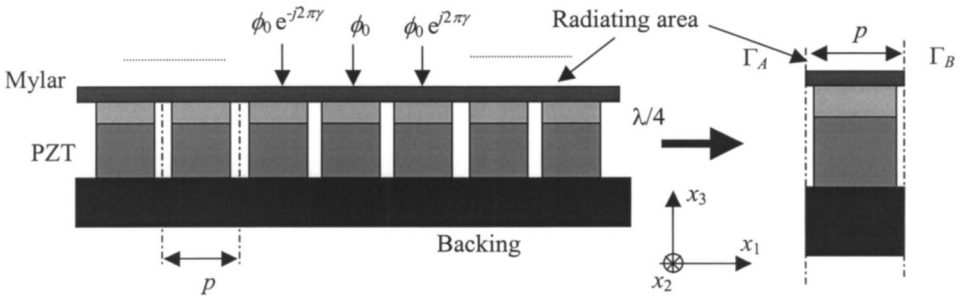

FIG. 1. Definition of the elementary cell of the considered transducer array, composed of PZT bars glued on a backing, with a matching layer, and covered with a Mylar layer.

ciency of the proposed approach, but the corresponding developments apply for any kinds of problems in the field of linear elasticity.

Moreover, the computation of harmonic admittance gives access to the mutual admittances and so to the cross-talk effects. Kino[16] first gave an analytical formulation of crosscoupling in the case of a classical transducer array (PZT bars on a backing). More recently, Certon *et al.*[17] measured cross-coupling effects in the case of a 1-3 piezocomposite array and they considered the piezocomposite as a homogeneous medium in their theoretical approach. Finally, the concept of mutual admittances[15] was introduced and is now adapted to transducer arrays. This latter formulation allows one to derive mutual admittances from the harmonic admittance and gives the practical conditions to be applied to perform electrical measurements of cross-talk effects. Using FEA, complex geometries of the structure and piezoelectricity are taken into account.

The basic principles of the simulation of periodic devices using FEA are summarized in Sec. II (following Ref. 14), together with very important notions such as harmonic and mutual admittances which we extensively use to characterize periodic transducers. We have implemented them to model standard multilayer (backing/PZT/matching layer) ultrasound transducers, and piezocomposite materials of 2-2 (1D periodic) and 1-3 (2D periodic) connectivity. For classical transducers, a comparison between different simple phase excitation conditions is conducted using nonperiodic and periodic computations. The capability of both approaches to accurately simulate actual operating conditions is then discussed. An illustration of the interest of periodic calculations is outlined, demonstrating the influence of undercuts in the backing on the guiding of lateral modes by the array. In the case of 2-2 connectivity composites, a comparison between nonperiodic and periodic computations of mutual admittance is reported. Mutual admittances for the very first neighbors of one excited period are computed and compared to those deduced from a Fourier transform of the harmonic admittance.[15] This leads to the definition of the minimum number of periods for which periodic computations can be trustfully considered. Results are also reported for 1-3 piezocomposite and compared to published data. As a conclusion, the use of such numerical tools for industrial design is discussed.

II. FINITE ELEMENTS APPLIED TO PERIODIC STRUCTURES

The development of finite-element calculations to address piezoelectricity problems has been reported in many articles (see e.g., Refs. 7–12). The description adopted for the present work relies on a mechanical displacement and electrical potential formulation[12–14] and only the final form of the problem is recalled here. Let us consider an elementary cell of a quasiperiodic transducer whose geometry conforms to the representation of Fig. 1. The operating behavior of this element without any acoustic load (in a vacuum) is considered here. One of the boundary conditions consists in the electrical excitation of the piezoelectric layer, which is assumed to be governed by an harmonic relation[15]

$$\phi_n = \phi_0 \exp(j2\pi n\gamma), \tag{1}$$

meaning that the nth active electrode is excited by a potential of magnitude ϕ_0 modulated by a phase proportional to its distance from the 0th electrode. The excitation parameter γ describes the way the structure is excited. For instance, an integer value of γ corresponds to a synchronous excitation, whereas $\gamma=1/2$ holds for an alternate $+V/-V$ excitation of the array. The bottom electrode is set to the reference potential (0 V). In the harmonic excitation frame, the mechanical displacements and the stresses obey a quasiperiodicity law

$$\begin{aligned} u_i(x_1+np) &= u_i(x_1)e^{j2\pi\gamma n} = u_{i_n}(x_1), \\ T_{ij}(x_1+np) &= T_{ij}(x_1)e^{j2\pi\gamma n} = T_{ij_n}(x_1). \end{aligned} \tag{2}$$

These relations yield specific boundary conditions at the limits Γ_A and Γ_B of the elementary cell of Fig. 1. These conditions are straightforwardly deduced from Eqs. (1) and (2) as shown in Eq. (3), and directly involve the degrees of freedom (DOF) at the corresponding boundary

$$\begin{Bmatrix} u_{\Gamma_B} \\ \phi_{\Gamma_B} \end{Bmatrix} = \begin{Bmatrix} u_{\Gamma_A} \\ \phi_{\Gamma_A} \end{Bmatrix} e^{j2\pi\gamma}. \tag{3}$$

Note that the spatial distribution of nodes (supporting the DOF) on Γ_A and Γ_B must be identical to ensure the coherence of Eq. (3). This relation is then used according to Ref. 14 to simplify the linear algebraic system obtained after discretization and integration of the piezoelectric Lagrangian expression.[12–14] Equation (3) imposes that the number of independent variables of the problem is reduced. However, in the present work, the initial number of DOF is preserved to avoid matrix reorganization, considered here as a source of

time consumption and yielding too many program complications. In this approach, a transformation matrix $[C_u]$ is introduced as

$$\begin{Bmatrix} u,\phi_{\Gamma_A} \\ u,\phi_{\Omega} \\ u,\phi_{\Gamma_B} \end{Bmatrix} = [C_{u,\phi}] \begin{Bmatrix} v,\varphi_{\Gamma_A} \\ v,\varphi_{\Omega} \\ v,\varphi_{\Gamma_B} \end{Bmatrix} = \begin{bmatrix} I_\Gamma & 0 & 0 \\ 0 & I_\Omega & 0 \\ I_\Gamma e^{j2\pi\gamma} & 0 & I_\Gamma \end{bmatrix} \begin{Bmatrix} v,\varphi_{\Gamma_A} \\ v,\varphi_{\Omega} \\ v,\varphi_{\Gamma_B} \end{Bmatrix}, \tag{4}$$

where u,ϕ_Ω are the DOF of the inner meshed domain (Γ_A and Γ_B excluded). Equation (4) is then inserted in the standard discrete form of FEA written as follows for a monochromatic dependence of mechanical and electrical fields [time dependence of the form $\exp(j\omega t)$]:

$$\begin{bmatrix} C_u^* & 0 \\ 0 & C_\phi^* \end{bmatrix}^t \begin{bmatrix} K_{uu}-\omega^2 M_{uu} & K_{u\phi} \\ K_{\phi u} & K_{\phi\phi} \end{bmatrix} \begin{bmatrix} C_u & 0 \\ 0 & C_\phi \end{bmatrix} \begin{Bmatrix} \nu \\ \varphi \end{Bmatrix} = \begin{bmatrix} C_u^* & 0 \\ 0 & C_\phi^* \end{bmatrix}^t \begin{Bmatrix} F \\ Q \end{Bmatrix}, \tag{5}$$

where K_{uu} and M_{uu} are, respectively, the stiffness and mass matrices of the purely elastic part of the problem, $K_{u\phi}$ is the piezoelectric coupling matrix, and $K_{\phi\phi}$ represents the purely dielectric part of the generalized piezoelectric stiffness matrix K. Superscripts t and * denote, respectively, matrix transposition and complex conjugation. Equation (5) is solved by setting $v_{\Gamma B}$ and $\varphi_{\Gamma B}$ to zero in order to comply with boundary condition (3). In the right-hand side of Eq. (5), F and Q are, respectively, relative to nodal mechanical and electrical load. These terms vanish within the meshed domain but can take nonzero values at its bounds, depending on the boundary conditions. One should note that in the case of complex matrices K_{uu}, $K_{u\phi}$, and $K_{\phi\phi}$, the matrix product on the left-hand side of Eq. (5) yields a general complex matrix with no particular symmetry but a large number of zeros. As a consequence, one can advantageously use a sparse matrix resolution algorithm[18] to reduce the computation time without loss in accuracy.

In the case of 3D computations with two periodic boundary conditions (see Fig. 2), one has to take particular care in the way the corners of the mesh are related to one another (see Ref. 14). In that case, the transformation matrix is written

$$\begin{Bmatrix} u,\phi_{\Gamma_A} \\ u,\phi_{\Gamma_C} \\ u,\phi_{\Omega} \\ u,\phi_{\Gamma_B} \\ u,\phi_{\Gamma_D} \\ u,\phi_{E_1} \\ u,\phi_{E_2} \\ u,\phi_{E_3} \\ u,\phi_{E_4} \end{Bmatrix} = [C_{u,\phi}] \begin{Bmatrix} v,\varphi_{\Gamma_A} \\ v,\varphi_{\Gamma_C} \\ v,\varphi_{\Omega} \\ v,\varphi_{\Gamma_B} \\ v,\varphi_{\Gamma_D} \\ v,\varphi_{E_1} \\ v,\varphi_{E_2} \\ v,\varphi_{E_3} \\ v,\varphi_{E_4} \end{Bmatrix} = \begin{bmatrix} I_{\Gamma_1} & & & & & & & & \\ 0 & I_{\Gamma_2} & & & & & & & \\ 0 & 0 & I_\Omega & & & & & & \\ I_{\Gamma_1} e^{j2\pi\gamma_1} & 0 & 0 & I_{\Gamma_1} & & & & & \\ 0 & I_{\Gamma_2} e^{j2\pi\gamma_2} & 0 & 0 & I_{\Gamma_2} & & & & \\ & & & & & I_E & & & \\ & & & & & I_E e^{j2\pi\gamma_1} & I_E & & \\ & & 0 & & & I_E e^{j2\pi\gamma_2} & 0 & I_E & \\ & & & & & I_E e^{j2\pi(\gamma_1+\gamma_2)} & 0 & 0 & I_E \end{bmatrix} \begin{Bmatrix} v,\varphi_{\Gamma_A} \\ v,\varphi_{\Gamma_C} \\ v,\varphi_{\Omega} \\ v,\varphi_{\Gamma_B} \\ v,\varphi_{\Gamma_D} \\ v,\varphi_{E_1} \\ v,\varphi_{E_2} \\ v,\varphi_{E_3} \\ v,\varphi_{E_4} \end{Bmatrix}, \tag{6}$$

where γ_1 and γ_2 are the two excitation parameters corresponding to the two directions of periodicity.

Considering the 2D computation case, inserting Eq. (3) into the discrete FEA formulation via the transformation matrix given by Eq. (4) makes the problem dependent on ω and γ. Thus, Eq. (5) must be solved for each couple (ω,γ) to determine the specific properties of a given structure, and particularly to calculate the harmonic admittance $Y(\omega,\gamma)$.[15] Since the magnitude of the excitation ϕ_0 is fixed to 1 V, $Y(\omega,\gamma)$ is directly given by the current generated in the active electrode by the vibration of the structure. This current is simply derived from the nodal charges on the active electrode using

$$Y(\omega,\gamma) = I(\omega,\gamma) = j\omega \sum_{n=1}^{Ne} Q_n, \tag{7}$$

where Ne is the total number of nodes at the considered electrode. One could also proceed as proposed by Lerch[12] by applying a constant charge excitation on the active electrode and then computing the resulting potential, directly providing the harmonic impedance for a unit charge excitation. This latter approach does not require the computation of the right-hand side of Eq. (5), but it does require either reorganize the stiffness and mass matrices (because the number of independent DOF is reduced) or to introduce one more transformation matrix. The first approach was preferred for imple-

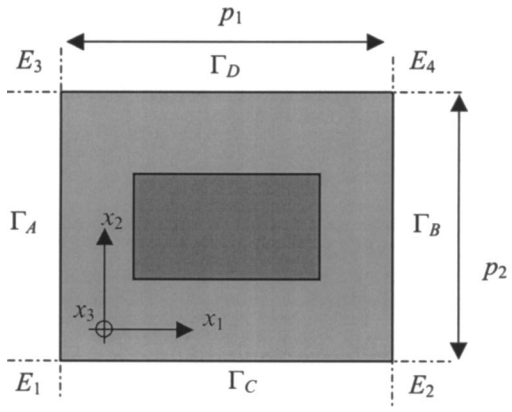

FIG. 2. In-plane definition of an elementary cell in the case of a biperiodic structure for 3D computations.

mentation in our computer software architecture. Using the harmonic admittance as defined in Eq. (7), one can easily define the mutual admittances[15] of the array by using the Fourier series property

$$Y_n(\omega) = \int_0^1 Y(\omega, \gamma) e^{j2\pi\gamma n} d\gamma. \tag{8}$$

Equation (8) describes the influence of one excited cell in the array (taken to be $n=0$) on the other cells, yielding, e.g., an estimate for the level of crosstalk between two adjacent cells or revealing propagation phenomena at the surface of the array along the x_1 axis (Fig. 1). The integral in Eq. (8) is evaluated using Gauss quadrature for γ defined in the range [0;0.5], taking advantage of the symmetry of the harmonic admittance around 0.5. For each frequency point, the computation of $Y_n(\omega)$ requires only the evaluation of $Y(\omega, \gamma)$ at the integration points, and the computational burden is low. This approach is very efficient for smooth contributions to the harmonic admittance. For sharp peaks, the proposed computation is valid only for a given range of neighbor cells. Since it is very difficult to define an equivalent degree of polynomial for such rapid variations of the harmonic admittance, this range cannot be rigorously defined and has to be determined empirically as shown in the next section.

In the case of 2D periodic structures (3D computations), two excitation parameters have to be considered which yield the following generalization for the mutual admittances

$$Y_{nm}(\omega) = \int_0^1 \int_0^1 Y(\omega, \gamma_1, \gamma_2) e^{j2\pi\gamma_1 n} e^{j2\pi\gamma_2 m} d\gamma_1 d\gamma_2. \tag{9}$$

III. COMPUTATION RESULTS AND ASSESSMENTS

A. Standard one-dimensional acoustic probe

The first case discussed in this section is that of classical 1D acoustic probes composed of PZT ridges on a backing with a matching layer, the whole structure being covered by a Mylar layer (as pictured in Fig. 1). The mesh used for the analysis is shown in Fig. 3. All computations are performed using second-order interpolation polynomials. The backing thickness is set to 1 mm and the PZT layer thickness as well.

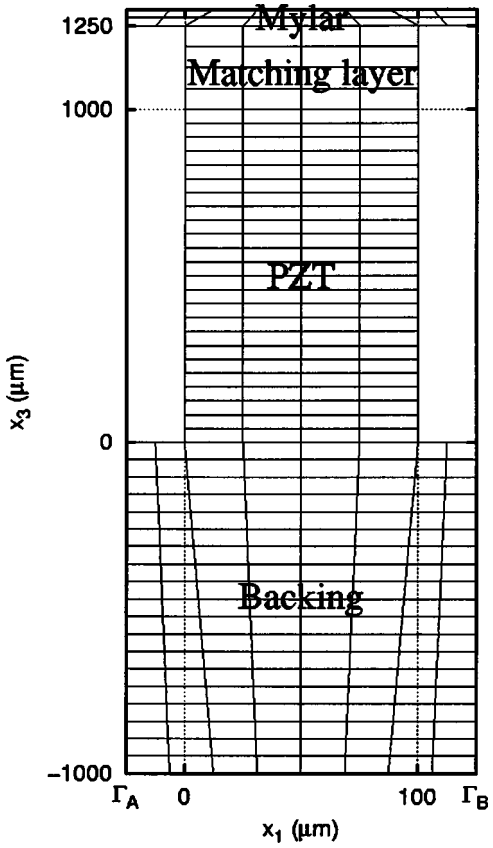

FIG. 3. Mesh of one cell of the considered periodic classical acoustic probe. The period is set to 150 μm.

The backing exhibits large acoustic losses (mechanical $Q=1.6$), while the acoustic and dielectric losses of the PZT layer, represented by the imaginary part of the material constants, are set to 1% of the real part of the material constants. The acoustic impedance of the matching layer is close to that of water, resulting in a layer thickness equal to 250 μm, with acoustic losses set to 10% of the elastic constants. The Mylar layer is 50 μm thick, with acoustic properties equivalent to those of the matching layer. This structure corresponds to an academic problem used only to assess the proposed analysis.

The computations were first performed assuming no periodic boundary conditions. Displacements along x_1 at the Γ_A and Γ_B boundaries are blocked in order to simulate adjacent cells. Only one phase arrangement can be considered in that case for transducer excitation. It is the synchronous operation of the infinite array (all cells are excited in phase), requiring one to mesh only one cell of the array. The periodic computation is then performed along the same lines, setting the excitation parameter γ to zero. The results are compared in Fig. 4. The perfect agreement between nonperiodic and periodic computations can be observed for $\gamma=0$, demonstrating that both calculations are equivalent ($u_1^{\Gamma_A} = u_1^{\Gamma_B} = 0$, $u_2^{\Gamma_A} = u_2^{\Gamma_A}$).

Another computation was then performed to illustrate how the proposed periodic computation can be used to qualitatively optimize periodic arrays. The well-known case of undercuts in the backing[17] is considered here. Figures 5(a) and 5(b) display the harmonic charge versus γ and ω for the

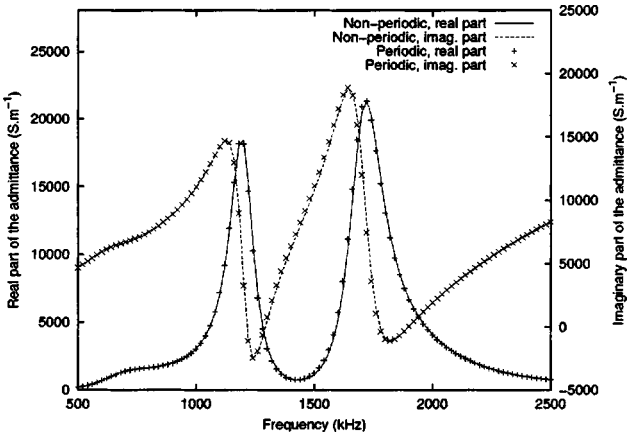

FIG. 4. Comparison between nonperiodic and periodic computations for the standard 1D acoustic probe of Fig. 3 operating in a vacuum.

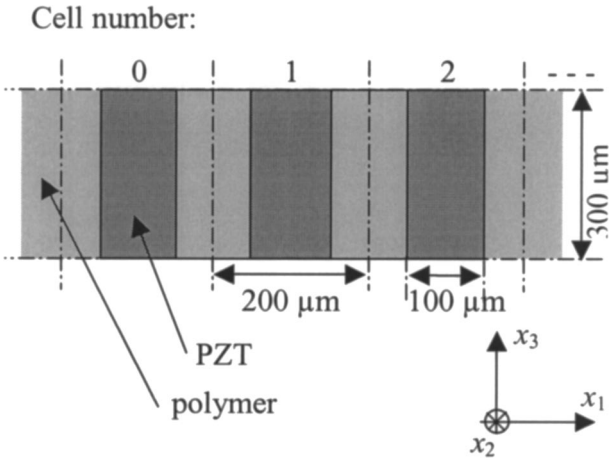

FIG. 6. Definition of the 2-2 connectivity piezocomposite material used for 2D computations. PZT and polymer bars are assumed infinite along the x_2 axis.

array of Fig. 1 without and with undercuts in the backing (undercut depth set to 200 μm). The harmonic charge is preferred for these plots because it allows a better illustration of the studied phenomena. The influence of the undercut clearly appears at low frequencies (under the first longitudinal resonance located at 1.5 MHz), causing the vanishing of large contributions to the harmonic charge that are due to propagation at the surface of the backing. One can numerically estimate the efficiency of the undercut by computing the solution of the problem for f=0.6 MHz and γ=0.5 where a large unwanted contribution to the harmonic charge is found. This effect is still present in the undercut structure but the displacements along x_1 (propagation direction) and x_3 (nor-

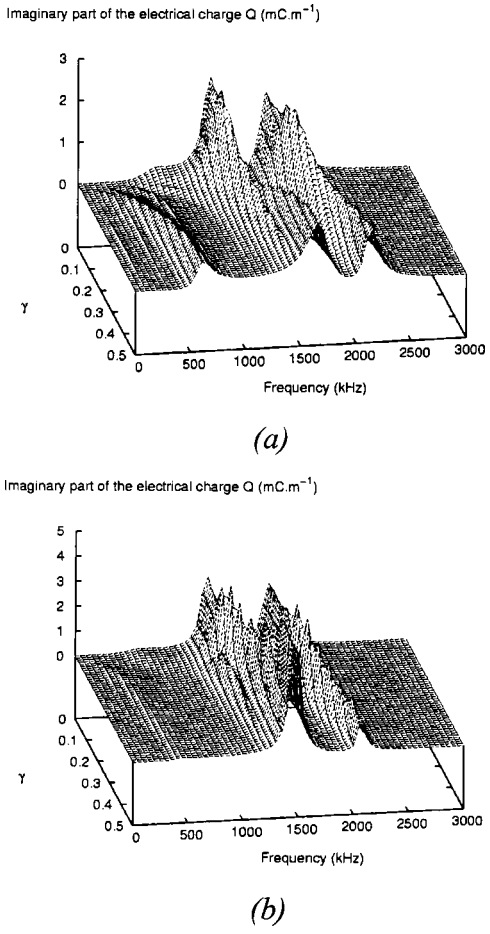

FIG. 5. Imaginary part of the harmonic electrical charge vs the excitation parameter γ and the angular frequency ω (a) without undercut and (b) with a 200 μm deep undercut. A spurious contribution to the electrical charge at low frequencies, corresponding to waves propagating at the surface of the backing, is strongly reduced.

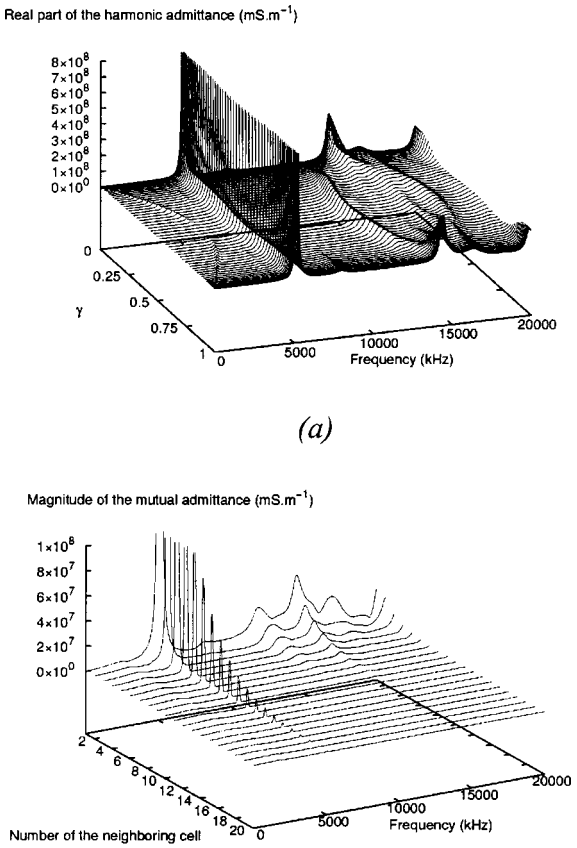

FIG. 7. Harmonic (a) and mutual (b) admittances for the 2-2 piezocomposite of Fig. 6.

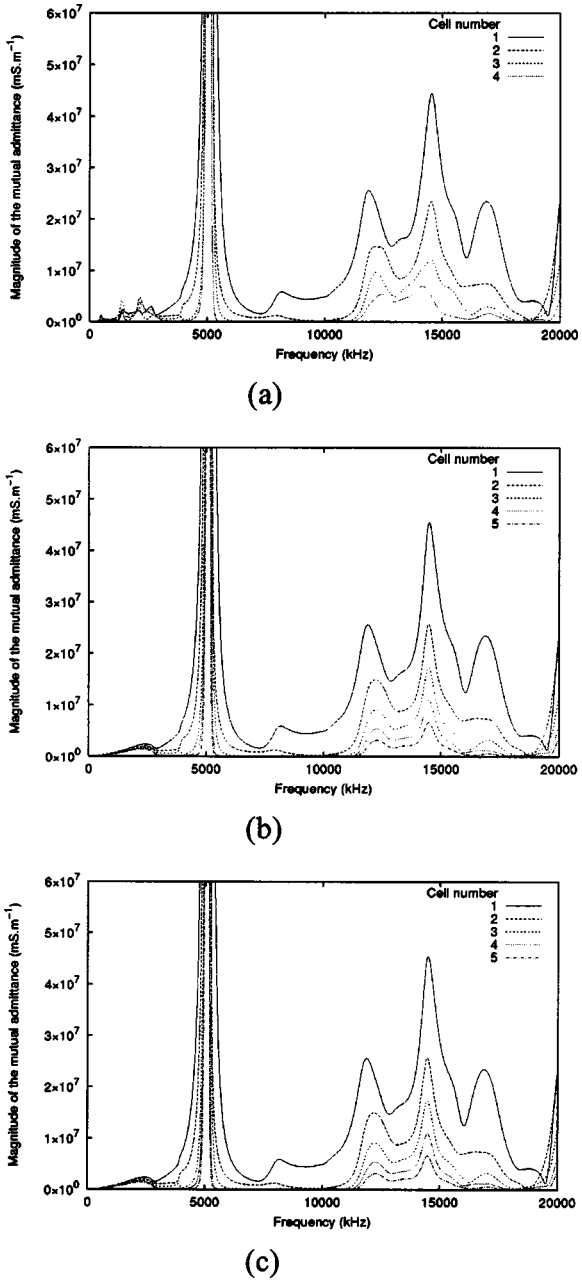

FIG. 8. Comparison between the mutual admittances of (a) a 9-cell finite length transducer, (b) a 49-cell finite length transducer, and (c) a periodic infinite 2-2 piezocomposite transducer. The electrical excitation is applied to cell 0. The mutual admittances of the 49-cell and the infinite devices exhibit a perfect agreement, considering the first five neighboring cells.

mal to the backing) are reduced, respectively, by a factor of 4 and 6 in magnitude when compared to the standard device.

B. 2-2 connectivity piezocomposite material

The case of 2-2 connectivity piezocomposites is now considered to illustrate the interest of the harmonic and mutual admittance concepts for the study of cross-talk effects. The geometry of the studied structure is depicted in Fig. 6. Once again, this is an academic problem of an infinite periodic transducer composed of infinitely long PZT and polymer bars perfectly glued together.

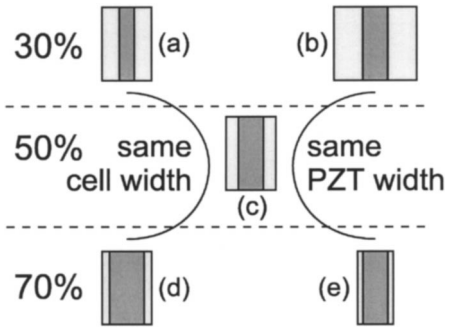

FIG. 9. Different combinations of 2-2 piezocomposite structure considered for a comparative analysis of their mutual admittances (a) 30% PZT vol. Fract. (w=60 μm, p=200 μm), (b) 30% PZT vol. Fract. (w=100 μm, p=333 μm), (c) 50% PZT vol. Fract., (d) 70% PZT vol. Fract. (w=140 μm, p=200 μm), and (e) 70% PZT vol. Fract. (w=100 μm, p=140 μm).

The mutual admittances [Eq. (8)] are computed using the Gauss integration procedure described in Sec. II. As indicated previously, due to the sharp variations of $Y(\omega,\gamma)$ for a transducer operating in a vacuum, a large number of integration points are required. The harmonic admittance is computed for 30 Gauss points with γ in the range [0;0.5]. Taking advantage of the symmetry of $Y(\omega,\gamma)$ around γ=0.5, this is equivalent to a numerical integration performed over 60 points. Figures 7(a) and 7(b) display $Y(\omega,\gamma)$ and the first 20 mutual admittances; for these the integration results are found to be reliable. Mutual admittances exceeding rank 20 exhibit sharp nonregular variations along ω caused by the instability of the numerical integration scheme along γ, resulting in artifacts. This sets a limitation to the proposed approach, the presented results corresponding to moderately sharp resonances (maximum quality factor smaller than the mechanical Q of the PZT set to 100 as in the previous section).

These results have also been assessed by comparing them with nonperiodic computations performed for 9-cell and 49-cell piezocomposite transducers. In both cases, only the central (n=0) cell is excited, all others being grounded. For a 1 V excitation, the nth mutual admittance is directly given by the current flowing between the electrodes of the nth cell. The results are plotted in Figs. 8(a)–8(c) for the 9-cell, the 49-cell, and the periodic structures, respectively. It clearly appears that the frequency dependence of the mutual admittances obtained in the three cases is very similar. The periodic and the 49-cell curves are almost indistinguishable. The most obvious differences are found when comparing the 9-cell mutual admittances to the two others. First, below the fundamental longitudinal mode of the transducer located at 5 MHz, a couple of small contributions arise, possibly due to structural resonances of the whole device (the length of the piezocomposite is 1.8 mm). The number of such low-frequency contributions increases with the number of cells considered in the computation while their magnitudes decrease. For the 49-cell device as well as for the periodic device, a kind of continuum of modes at the corresponding frequencies can be observed. In the vicinity of the fundamental longitudinal mode, almost no differences arise between the three computations. The most representative deviations

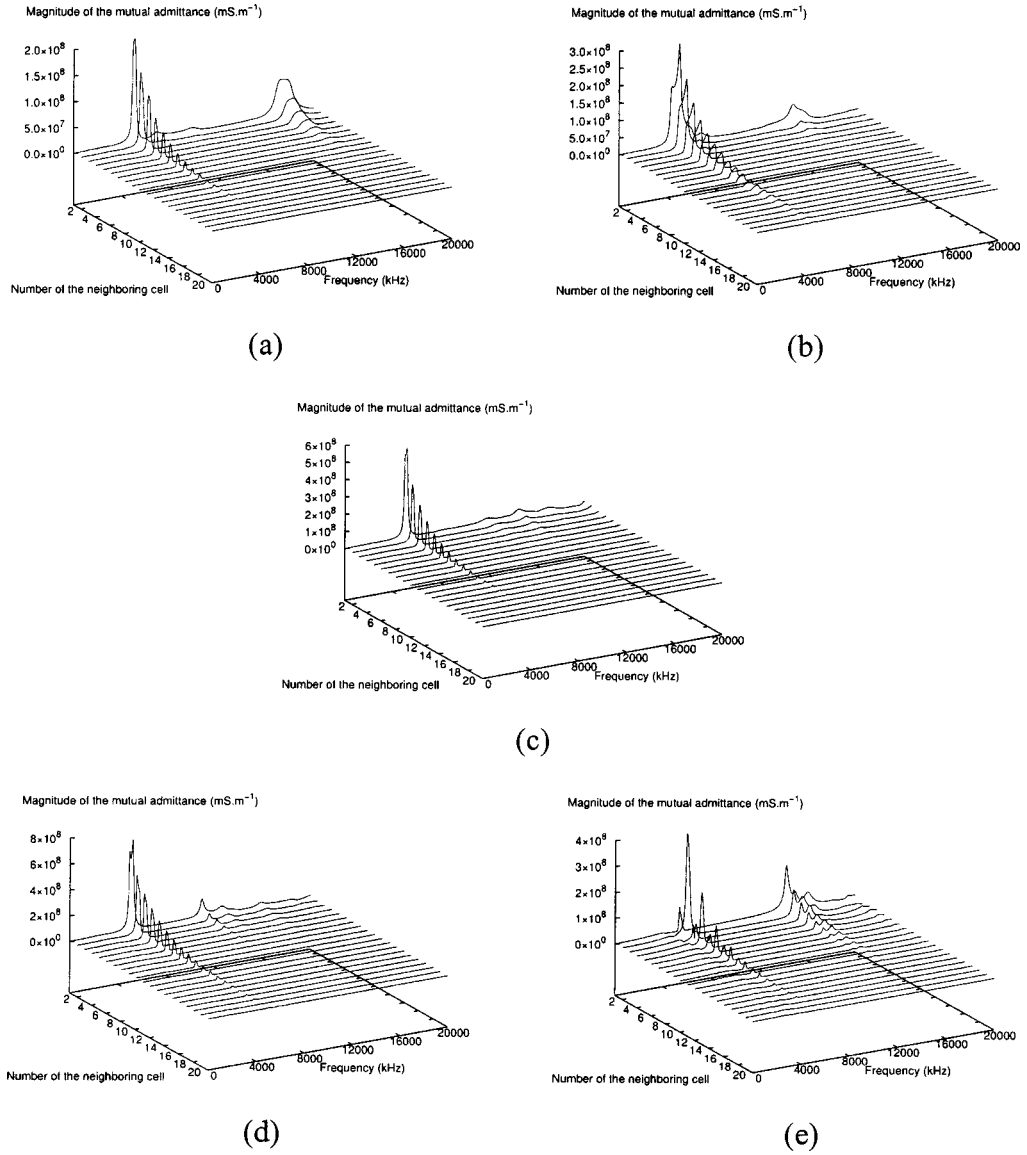

FIG. 10. (a)–(e) Mutual admittances for the five configurations of Fig. 9.

are found at frequencies above 10 MHz at which contributions due to lateral modes, Lamb modes, and the third overtone of the fundamental mode overlap. The mutual admittances of the 9-cell device exhibit frequency dependences that are more difficult to analyze than the two other cases, certainly due to the influence of the boundary conditions. Again, it can be remarked that for the first two neighbors of the excited cell, the three results are very close. As a conclusion for these 2D computations, even moderately long arrays (i.e., larger than ten periods) can be efficiently analyzed using periodic FEA.

The computation of mutual admittance has also been performed for various combinations of PZT and polymer volumes within the considered cell to check the capability of our approach to identify specific behavior of the different corresponding 2-2 piezocomposite structures. Volume fractions of PZT equal to 30% and 70% have been imposed assuming either a constant period (200 μm), or a constant width of the ridge (100 μm), the thickness of the structure remaining fixed to 300 μm. Figure 9 shows the considered arrangements of 2-2 piezocomposite and the calculation results are reported in Fig. 10, compared to the mutual admittances of the 50% PZT volume fraction device previously considered.

In terms of magnitude and modal purity of the mutual admittance, Fig. 10(a) for which the width/thickness ratio (*w/t*) is the smallest (0.2) exhibits the most advantageous response. As a counterpart, only a small volume of the cell contributes to the useful longitudinal vibration, which also explains the small amount of cross-talk effects related to this mode. However, one can point out a large contribution of the first lateral mode on the first neighbor mutual admittance. For this mode, the vibration mainly takes place within the polymer. Since Fig. 10(a) exhibits the largest amount of polymer among all those regarded, it is rather easy to explain the observed result. For Fig. 10(b), this mode is found to strongly contribute to the first neighbor mutual admittances. Figure 10(b) also exhibits large cross-talk effects in terms of propagation depth along the grating. Figure 10(d) for which the *w/t* is close to 0.5 provides the largest fundamental lon-

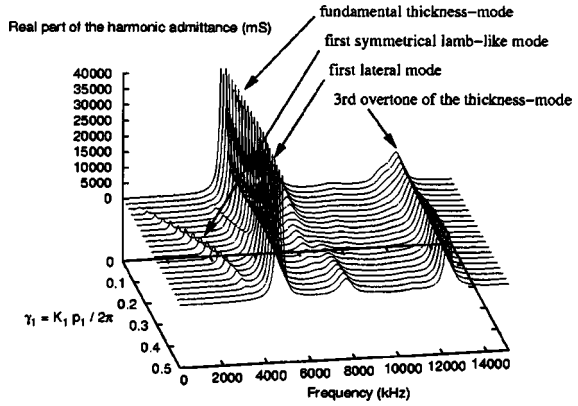

FIG. 11. Real part of the harmonic admittance of the considered 1-3 connectivity piezocomposite (biperiodic structure) for $\gamma_2=0$ and γ_1 varying from 0 to 0.5.

gitudinal vibration, but also a very large amount of cross-talk phenomena, with important contributions of Lamb wavelike modes. Figure 10(e) shows a complicated distribution of mutual admittances, with large contributions for even neighbors and smaller responses for odd ones. Furthermore, low-order Lamb wavelike modes seem to interact with the piston mode. The largest third overtone contributions are also found in that case, mixed with higher-order modes.

Finally, a tradeoff can be reached with Fig. 10(c). Even if lateral mode contributions occur, it is the one which exhibits the smallest cross-talk phenomena related to the first longitudinal mode. On the other hand, it is clear that precise criteria have to be defined to select one or the other solution. Whatever these criteria could be, it is shown that different configurations of 2-2 piezocomposite yield different mutual admittance figures which can be actually used to accurately optimize the structure.

C. 1-3 connectivity piezocomposite—three-dimensional computations

The computation of 2D periodic structures was also implemented to analyze 1-3 connectivity piezocomposite properties. The first studied piezocomposite exhibits two periods of 200 μm and a thickness of 300 μm, the volume fraction being set to 1/4. In this calculation, the harmonic admittance depends on the angular frequency and on the two propagation parameters γ_1 and γ_2. First computations to validate the approach were performed by setting γ_2 to zero and scanning γ_1 from 0 to 0.5. The different modal contributions showing out in the harmonic admittance (see Fig. 11) have then been identified. The first mode is the first symmetrical Lamb-type wave clearly exhibiting a frequency stopband (well identified in literature). The fundamental longitudinal mode is then naturally found, and then the first lateral mode for γ_1 smaller than 0.3. The third overtone is also easily identified. The observed dispersion behavior is very close to that of the previous section [compare Fig. 7(a) with Fig. 11] This result was expected since all cells along x_2 are assumed to vibrate synchronously, an operating principle very close to that of 2-2 piezocomposite devices. Note that

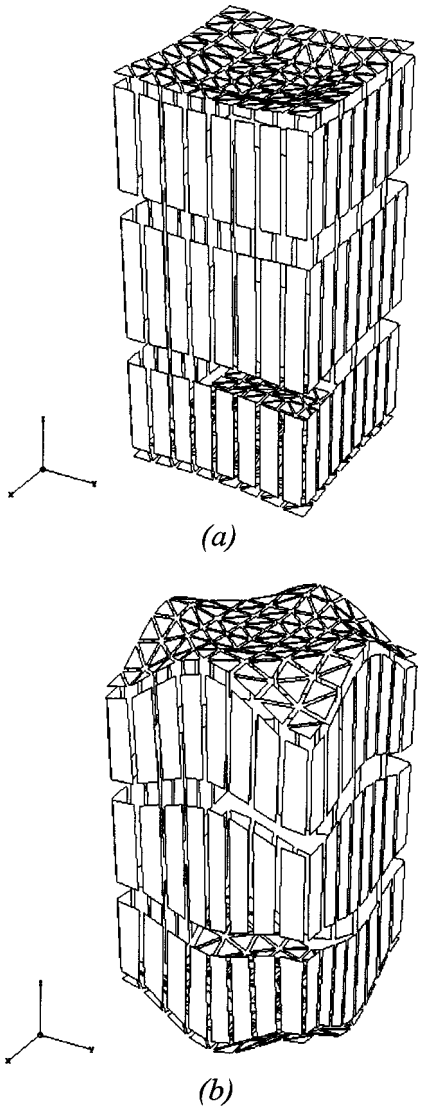

FIG. 12. Displacement fields of the fundamental thickness mode (a) and the first lateral mode (b) located in Fig. 9 with $\gamma_1=\gamma_2=0$. In the case of the first lateral mode, the polymer and the PZT do not vibrate synchronously; moreover, the polymer exhibits a larger magnitude of vibration than the PZT.

inverting γ_1 and γ_2 in the calculation scheme yields the same results since the structure is symmetric (square in-plane section of the period).

It can be remarked that the resonant frequency and the magnitude of the fundamental longitudinal mode are both affected by the value of γ_1. The corresponding dependence can be rigorously identified using the approach proposed in Ref. 19. Figures 12(a) and 12(b) show the displacement fields for two values of the frequency corresponding, respectively, to the fundamental longitudinal mode and the first lateral mode (considering $\gamma_1=\gamma_2=0$), this latter being due to Bragg diffraction of transverse waves in the periodic structure.[20,21]

Finally, mutual admittances were computed for a 1-3 piezocomposite structure exhibiting a volume fraction of 0.55, two periods of 600 μm, and a thickness of 900 μm. The width of the square section PZT bar is 445 μm. In that case, one has to compute many more values of the harmonic ad-

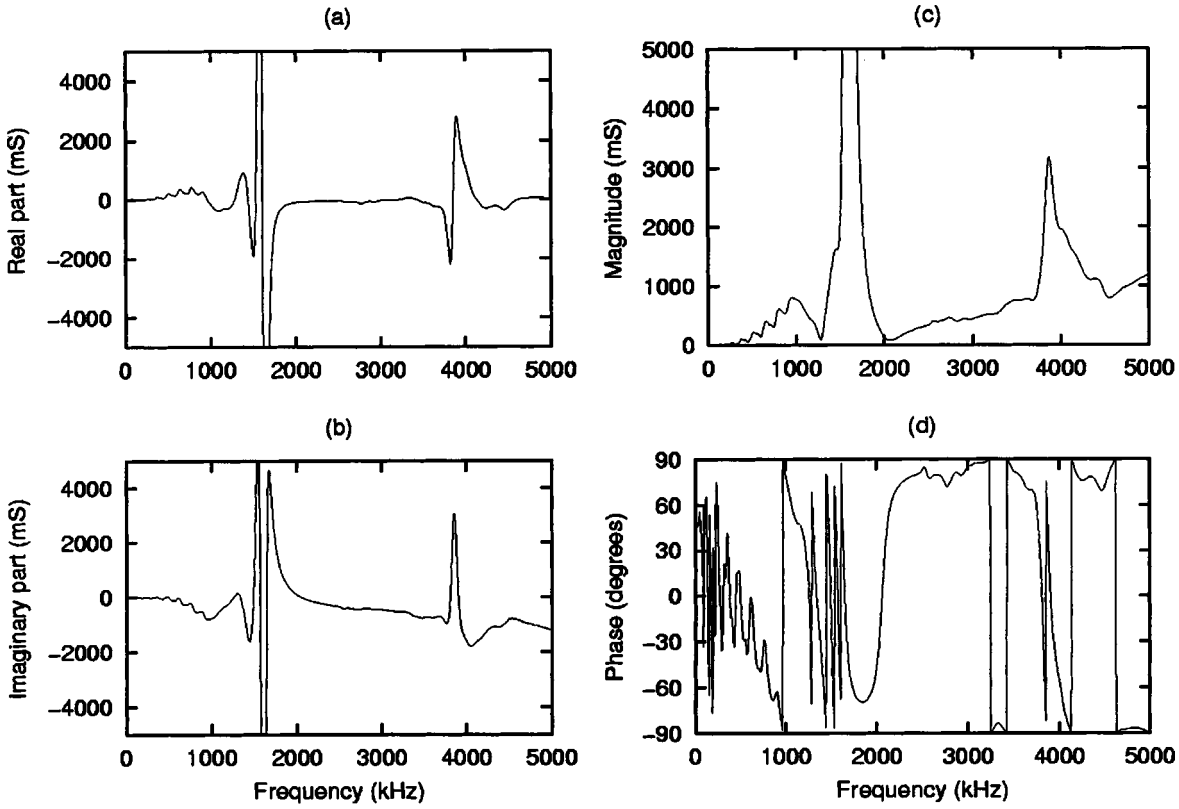

FIG. 13. Mutual admittance of the first neighbor of the excited cell along the x_1 direction, for the considered 1-3 connectivity piezocomposite. Real (a) and imaginary (b) parts, as well as the magnitude (c) and the phase (d) are shown. The continuum of modes at low frequencies is due to the S0-Lamb-type mode of the structure, whose cutoff frequency is approximately 1 MHz.

mittance to achieve a good accuracy for the Gauss integration scheme. In the present case, the number of Gauss points along γ_1 and γ_2 was restricted to 13 (169 calculation points for each value of ω) and the number of frequency points to 501.

Figure 13 shows the mutual admittance of the first neighbor of the excited cell along the x_1 axis. At low frequencies, the kind of continuum of modes is due to the contribution of the S0-Lamb-type mode whose cutoff frequency is about 1 MHz. A similar contribution was measured by Certon *et al.*[17] for 1-3 piezocomposite arrays. Finally, the contributions of the fundamental thickness mode and its third overtone are easily found at 1.6 MHz and 3.9 MHz, respectively.

IV. CONCLUSION

A calculation method for the simulation of periodic structures using the finite-element method has been developed and implemented to analyze the properties of periodic transducer arrays. The method has been tested for different kinds of transducers (classical stacked transducers, 2-2 and 1-3 connectivity piezocomposite materials). Particularly, the extensive use of mutual admittances provides an evaluation of cross-talk effect which could be useful for the design of high-quality transducers for imaging applications and nondestructive evaluations. Indeed, the influence of fine changes in a given structure (geometry, materials) on the magnitude of mutual admittances can be directly evaluated, which can be used to identify the best transducer configuration according to the amount of permitted crosstalk.

ACKNOWLEDGMENTS

The authors thank J. Desbois for many fruitful discussions concerning pseudoperiodic problems and their modeling.

[1] W. P. Mason, *Physical Acoustics* (Academic, New York, 1964), Vol. 1, Part A.
[2] *Handbook of Physics* (Academic, New York, 1962).
[3] P. Lloyd and M. Redwood, J. Acoust. Soc. Am. **39**, 346 (1966).
[4] R. Holland, IEEE Trans. Sonics Ultrason. **15**, 97 (1968).
[5] H. F. Tiersten, Proc. IEEE **55**, 1523 (1967).
[6] E. P. Eernisse, IEEE Trans. Sonics Ultrason. **14**, 153 (1967).
[7] H. Allik and T. J. R. Hugues, Int. J. Numer. Methods Eng. **2**, 151 (1970).
[8] H. Allik, K. M. Webman, and J. T. Hunt, J. Acoust. Soc. Am. **56**, 1782 (1974).
[9] D. Boucher, Y. Lagier, and C. Maerfeld, IEEE Trans. Sonics Ultrason. **28**, 318 (1981).
[10] M. Naillon, R. H. Coursant, and F. Besnier, Acta Electron. **25**, 341 (1983).
[11] W. Steichen, G. Vanderbork, and Y. Lagier, *Power Sonics and Ultrasonics Transducer Design* (Springer, Berlin, 1988), p. 160–174.
[12] R. Lerch, IEEE Trans. Ultrason. Ferroelectr. Freq. Control **37**, 233 (1990).
[13] B. T. Khury-Yakub, F. L. Degertekin, X.-C. Jin, S. Calmes, I. Ladabaum, S. Hansen, and X. J. Zhang, Proceedings of the IEEE Ultrasonics Symposium, Sendai, Miyagi, Japan, October 5–8, 1998, pp.985–992.
[14] P. Langlet, A. C. Hladky-Hennion, and J. N. Decarpigny, J. Acoust. Soc. Am. **98**, 2792 (1995).
[15] Y. Zhang, J. Desbois, and L. Boyer, IEEE Trans. Ultrason. Ferroelectr. Freq. Control **40**, 183 (1993).

[16] G. S. Kino and R. Baer, Proceedings of the IEEE Ultrasonics Symposium, Atlanta, Georgia, October 31–November2, 1983, pp. 1013–1019.
[17] D. Certon, N. Felix, E. Lacaze, F. Teston, and F. Patat, IEEE Trans. Ultrason. Ferroelectr. Freq. Control **48**, 85 (2001).
[18] T. A. Davis and I. S. Duff, SIAM J. Matrix Anal. Appl. **18**, 140 (1997).
[19] S. Ballandras, P.-F. Edoa, F. Langrognet, W. Steichen, and G. Pierre, Proceedings of the IEEE Ultrasonics Symposium, San Juan, Puerto Rico, October 22–25, 2000, pp. 1139–1142.
[20] D. Certon *et al.*, J. Acoust. Soc. Am. **101**, 2043 (1997).
[21] D. Certon *et al.*, IEEE Trans. Ultrason. Ferroelectr. Freq. Control **44**, 643 (1997).